Three-dimensional assemblies of semiconductor quantum dots in a wide-gap matrix providing an intermediate band for absorption

Voicu Popescu and Alex Zunger

Articles you may be interested in

Inter-band optoelectronic properties in quantum dot structure of low band gap III-V semiconductors
J. Appl. Phys. **115**, 143107 (2014); 10.1063/1.4870939

Influence of wetting layers and quantum dot size distribution on intermediate band formation in InAs/GaAs superlattices
J. Appl. Phys. **110**, 073105 (2011); 10.1063/1.3631785

III-V compound semiconductor screening for implementing quantum dot intermediate band solar cells
J. Appl. Phys. **109**, 014313 (2011); 10.1063/1.3527912

Absorption characteristics of a quantum dot array induced intermediate band: Implications for solar cell design
Appl. Phys. Lett. **93**, 263105 (2008); 10.1063/1.3058716

Temperature dependence of intersublevel absorption in InAs/GaAs self-assembled quantum dots
Appl. Phys. Lett. **80**, 4620 (2002); 10.1063/1.1487446

Three-dimensional assemblies of semiconductor quantum dots in a wide-gap matrix providing an intermediate band for absorption

Voicu Popescu[1,2,a)] and Alex Zunger[3,b)]

[1]*Physics Department and REMRSEC, Colorado School of Mines, Golden, Colorado 80401, USA*
[2]*National Renewable Energy Laboratory, Golden, Colorado 80401, USA*
[3]*University of Colorado, Boulder, Colorado 80302, USA*

We consider a self-assembled quantum dot (QD) system consisting of the QD itself, the wetting layer and the matrix on a substrate. The electronic structure for various III-V material combinations was determined by atomistic empirical pseudopotential calculations. Taking the widely investigated InAs/GaAs/GaAs(001) system as benchmark, we analyze the changes induced in the energy levels and offsets relevant for a QD-based intermediate band solar cell (IBSC). We explore the effects of (i) the dot material, (ii) the matrix material, and (iii) dot-matrix-substrate combinations that may enable strain balanced structures. Using as unique reference criterion the relative position of the intermediate band inside the band gap of the matrix, we suggest the dot/matrix/substrate combinations InAs/(In,Ga)P/GaAs(001), In(As,Sb)/GaAs/InP(001), and InAs/Ga(As,Sb)/InP(001) as promising candidates for QD-IBSCs. © *2012 American Institute of Physics*. [http://dx.doi.org/10.1063/1.4767377]

I. INTRODUCTION

Photovoltaic solar cells utilizing a single absorbing material have usually used an absorber with a 1.3–1.5 eV band gap (close to the single-junction maximum efficiency), thus giving up the prospects of absorption at lower sub-band-gap, infrared frequencies. One way to avoid such a waste is to engineer a partially occupied energy band within the band gap of the primary absorber,[1] as sketched in Fig. 1(a). Absorption from the matrix valence band (VB) to such an intermediate band (IB), and from it to the matrix conduction band (CB) would then provide additional low-energy channels [the transitions labeled B and C in Fig. 1(a)] for creating useful carriers to the benefit of the collected solar cell current that is otherwise obtained solely as a result of the fundamental transition across the band gap [labeled A in Fig. 1(a)]. One way to affect such an IB is to consider quantum dots (QDs), embedded in a wider band gap matrix, in which case the IB will be formed by the QD-confined electron (or hole) levels, as illustrated in Fig. 1(b). A central issue here is to identify a combination of QD and matrix material that would position ideally the IB with respect to the matrix VB maximum (VBM) E_v and CB minimum (CBM) E_c. Such ideal positions stem from the various conditions that maximize the beneficial effects of the IB and minimization of the adverse effects.

Considering only those aspects related to the electronic structure of a typical QD-IBSC depicted in Fig. 1, we have formulated[2] several conditions needed to be fulfilled in order to maximize the gained efficiency from such a device as well as those deleterious processes that need to be curtailed. The needed requirements can be summarized as follows: (i) the VB → IB and IB → CB excitations must be optically allowed and strong; consequently, the agent creating the IB must have significant concentration and oscillator strength; (ii) the VB → IB and IB → CB absorption spectra should ideally have no spectral overlap with each other ("photon sorting" condition); (iii) the IB should be positioned at specific "target values" such as to separate the host band gap E_g into two parts E_H and E_L. Calculations for concentrated light[1] have shown that a maximum efficiency can be obtained for $E_L \simeq E_c - 0.7$ eV and $E_H \simeq E_v + 1.2$ eV or, conversely, $E_L \simeq E_c - 1.2$ eV and $E_H \simeq E_v + 0.7$ eV. Later on, Bremner *et al.*[3] solved the rate equations considering the standard terrestrial (Air Mass 1.5) solar spectrum and found that, in fact, several local maxima may appear in the quantum efficiency for a set of different (E_L, E_H) pairs, with values that are not too far from those given above.[3]

In the past few years, a number of attempts were made to grow III-V QDs in a matrix made of another III-V material, so as to create a system where the confined levels would
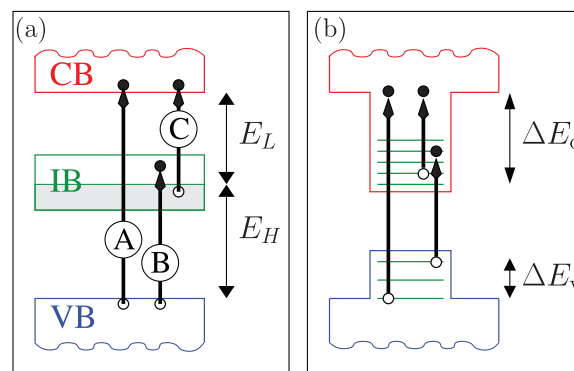
FIG. 1. (a) Schematic representation of the IBSC with the main transition (A) across the fundamental band gap and the additional, IB-mediated, low energy transitions (B) and (C); (b) the suggested QD IBSC implementation, with the IB formed by the QD-confined electron levels.

a)Present address: University of Duisburg-Essen, Faculty of Physics, Duisburg, Germany. E-mail: voicu.popescu@uni-due.de.
b)E-mail: alex.zunger@gmail.com.

TABLE I. Survey of several III-V QD-IBSC systems published so far.

QD material	Matrix	Substrate	Strain	Reference	Comments
InAs	GaAs	GaAs(001)	SK, strained	4 and 5	IB↦CB evidence
InAs	GaAs	GaAs(001)	SK, strain-balanced	6	GaP strain-compensating layers
				7	Ga(As,P) strain-compensation
InAs	GaAs	GaAs(001)	SK, strained	8	(Al,Ga)As "fence" structure
InAs	GaAs	GaAs(001)	SK, strained	17	"built-in charge"
InAs	Ga(As,Sb)	GaAs(001)	SK, strained	12 and 13	Sb $\leq$ 23%, $\Delta E_v = 0.0$
InAs	Ga(As,N)	GaAs(001)	SK, strain-balanced	9–11	N $\leq$ 4%, proof of radiative IB↦CB transition
In(As,Sb)	GaAs	GaAs(001)	SK, strained	14 and 15	IB formed by holes
GaSb	GaAs	GaAs(001)	IMF	16	IB formed by holes

satisfy the above conditions. The choice of the systems, however, has generally not been tuned to achieve the ideal target but was more often based on utilizing laboratory available III-V materials that were known to produce QDs in the Stranski-Krastanov (SK) growth-mode. Indeed, the paradigm system used most often—InAs dots in a GaAs matrix—was selected largely because it is a known QD system, not because it is supposed to create the IB in the right location. We summarize in Table I the III-V QD systems that were so far tried experimentally for achieving a QD-IBSC. This table shows the significant weight the aforementioned system, InAs/GaAs, has in the various attempts made to implement the QD-IBSC concept.[4,5] Indeed, most of the effort was put in improving the device quality by modifying the matrix through strain-compensating GaP and Ga(As,P) layers,[6,7] "fence" layers,[8] alloying the GaAs matrix with nitrogen[9–11] to relieve the strain, or with antimony[12,13] to improve the QD morphology. Alternatives to the InAs QD are quite rare, examples being In(As,Sb)[14,15] or GaSb.[16] In nearly all cases, the base system was still InAs/GaAs which is not optimal.[5] Disappointingly, in all of these cases, the insertion of QDs in the cells could at best match the open circuit voltage and quantum efficiency of the *reference* GaAs cell.

The atomistic theory of self-assembled semiconductor QDs has progressed during the last decade to the point of being an accurate predictive tool. It treats the electronic structure of a given three-dimensional (3D) geometrical arrangement of dots by solving the 3D Schrödinger equation that describes the confined energy levels generated by *atomistic pseudopotentials* (PPs) in a plane-wave basis. The pseudopotential approach avoids the effective mass and envelope function approximations, treating instead the QD and its matrix as a giant molecule. Inter-band as well as inter-valley coupling effects are thus naturally present. The Hamiltonian reflects the atomic-level symmetry of the dot (since atomic pseudopotentials are centered about atoms) as well as spin-orbit effects and the correct dot-matrix band offsets. Its diagonalization yields energy levels and wavefunctions. In this paper, we use this modern theory of nanostructures to examine a range of III-V materials for their ability to create an effective IB system. We change (i) the dot material, (ii) the matrix material, and (iii) explore dot-matrix-substrate combinations that allow strain balance. We calculate the confined energy levels keeping the dot shape at its standard form given by the SK growth

mode and use InAs dots in the GaAs matrix grown on GaAs(001) substrate as a reference (benchmark) system. The central quantities we are looking at are related to the band allignment, comparing the actual calculated values of E_L and E_H in each system with those predicted[1,3] to maximize the quantum efficiency. We also investigate several material combinations that allow for strain balance engineering of the QD-IBSC device. This is an important issue in the actual implementation, since a large number of QD layers are needed to form the solar cell: both in order to increase the amount of absorbed radiation and provide a sufficiently large flat-band region.[33] Amongst the surveyed systems, we find as promising candidates: (a) InAs dots embedded in the wide band-gap $In_{0.3}Ga_{0.7}P$ matrix; (b) In(As,Sb) dots in GaAs; and (c) InAs dots in Ga(As,Sb) matrix. These material combinations, combined with appropriate substrates, e.g., GaAs(001) for system (a) and InP(001) for (b) and (c) offer, in addition, the possibility of a strain-balance realization.

II. NEEDED CONDITIONS

We shall focus here on four main issues that, in fact, summarize the needed conditions given above.

1. The electron levels offset [ΔE_c in Fig. 1(b)] plays the role of E_L if the IB is to be formed by electron levels. In order to reduce the capture of matrix CB electrons by the IB, ΔE_c needs to be brought as close as possible to the ideal value $E_L = 0.7$ eV [requirement (iii)].

2. The hole levels offset ΔE_v needs to be minimized, ideally brought to zero. The reason for this requirement is that the open circuit voltage V_{oc} is effectively reduced by ΔE_v from its ideal value $E_g = E_c - E_v$, if matrix VB holes are trapped by the QD-confined hole states.

3. The inter-band transition (between confined holes or host VB and IB states) plays the role of E_H and, as stated by requirement (iii), should be as close as possible to its ideal value $E_H = 1.2$ eV.

4. It follows directly that we should look for $E_L + E_H \simeq 1.9$ eV to be fulfilled, which is either the band gap of the matrix (if $\Delta E_v \to 0$) or $E_c - E_v + \Delta E_v$.

We further note that, in the case of the IB formed by holes, the roles of ΔE_c and ΔE_v are simply reversed. In the following, each of our analysis of the various systems discussed will essentially follow the evolution of these

parameters (1) through (4) from case to case identifying positive or negative trends.

III. HOW ARE THE PROPERTIES OF 3D ASSEMBLIES OF SEMICONDUCTOR QUANTUM DOTS IN A MATRIX CALCULATED

Our main goal here is to establish the potential of several III-V materials combinations in providing the desired energy levels offset close to the ideal IBSC conditions. We have thus investigated a prototype system consisting of matrix, QD, and wetting layer (WL) with a fixed geometry. Our calculations rely on an atomistic description that is by now well established and has been presented in detail elsewhere.[18,19] It essentially consists of diagonalizing the Hamiltonian of a million-atom supercell decorated with the corresponding group III and V elements belonging to the matrix, QD, and WL materials. The main steps of the method, briefly discussed in the following, are: (i) setting up the structure using the zinc-blende unit cell as building block and optimizing the atomic positions; (ii) solving the eigenvalue problem for the QD; and (iii) determining the matrix electronic structure. In all our simulations, we use a lens-shaped QD of diameter $d = 25$ nm, height $h = 3.5$ nm, and a 2 monolayer (ML) thick WL. While periodic boundary conditions are used in solving the single-particle eigenvalue problem, the lateral and vertical dot-dot separations were taken large enough (25 nm) in order to ensure the decoupling of the dots and thus mimic the behavior of a single, isolated QD.

A. Atomic displacements in search of strain minimization

We first construct the supercell containing the QD, WL, and the matrix from unrelaxed bulk primitive cells, and then require that these are coherently strained by the substrate assuming the constraint of a common in-plane lattice constant for all the materials in the system. The supercell height is optimized along the growth direction and the atomic positions are further allowed to relax so as to minimize the total strain in the system. The relaxed geometry is obtained by minimizing the elastic strain energy calculated here using a valence force field (VFF) functional in its generalized form:[20–22]

$$E = \sum_i \sum_j^{nn\,i} \frac{3}{8}\alpha_{ij}\Delta d_{ij}^2 + \sum_i \sum_{k>j}^{nn\,i} \frac{3\beta_{jik}}{8d_{ij}^0 d_{ik}^0}$$
$$\times [(\vec{R}_j - \vec{R}_i)\cdot(\vec{R}_k - \vec{R}_i) - \cos\theta_{jik}^0 d_{ij}^0 d_{ik}^0]^2$$
$$+ \sum_i \sum_{k>j}^{nn\,i} \frac{3\sigma_{jik}}{d_{ik}^0}\Delta d_{ij}$$
$$\times [(\vec{R}_j - \vec{R}_i)\cdot(\vec{R}_k - \vec{R}_i) - \cos\theta_{jik}^0 d_{ij}^0 d_{ik}^0]. \quad (1)$$

In this equation, $\Delta d_{ij} = [(\vec{R}_i - \vec{R}_j)^2 - (d_{ij}^0)^2]/d_{ij}^0$, $\vec{R}_i$ is the coordinate of atom i, and d_{ij}^0 is the ideal (unrelaxed) bond distance between atoms i and j. Further, θ_{jik}^0 is the ideal (unrelaxed) angle of the bond j–i–k. The notation $\sum^{nn\,i}$ denotes summation over the nearest neighbors of atom i. The

TABLE II. Equilibrium lattice constant a_0, input VFF force constants α, β, σ entering Eq. (1) and the elastic constants C_{ij} used to derived these quantities for GaSb and InSb.

	a_0 (Å)	α	β (10^3 dyne/cm)	σ	C_{11}	C_{12} (10^{11} dyne/cm²)	C_{44}
GaSb	6.0959	26.30	7.330	−2.768	6.67	4.02	4.32
InSb	6.4794	18.70	4.892	−4.921	8.83	3.65	3.02

bond stretching, bond angle bending, and bond-length/bond-angle interaction terms are described by the VFF parameters α_{ij}, β_{ijk}, σ_{ijk}, which are related to the elastic coefficients C_{ij} of the corresponding bulk material.[22] In our present calculations, we have considered (In,Ga)(As,P,Sb) combinations with the VFF parameters for (In,Ga)Sb given in Table II while for the others materials—(In,Ga)(As,P)—those listed in Ref. 2.

B. Setting up the single-particle Schrödinger equation with atomic resolution

For each of the relaxed configurations, we solve[18,23] the single-particle equation

$$\left[-\frac{\beta}{2}\nabla^2 + \sum_{n,\alpha} \hat{v}_\alpha(\vec{r} - \vec{R}_{n\alpha}, \underline{\varepsilon}_n) + \hat{V}_{NL} \right]\psi_i(\vec{r}) = E_i\psi_i(\vec{r}). \quad (2)$$

Here, $\hat{V}_{NL}$ represents the non-local spin-orbit coupling potential, β (taken to be 1.23 throughout this work) a scaling factor for the kinetic energy,[23] while $\hat{v}_\alpha(\vec{r} - \vec{R}_{n\alpha}, \underline{\varepsilon}_n)$ is a screened atomic pseudopotential that depends on the identity α of the atom located at site n and the local strain $\underline{\varepsilon}_n$

$$v_\alpha(\vec{r}, \underline{\varepsilon}_n) = v_\alpha(\vec{r}, 0)[1 + \gamma_\alpha \text{Tr}(\underline{\varepsilon}_n)], \quad (3)$$

with γ_α a fitting parameter introducing a further dependence on the identity of the neighbors.[23] The unstrained pseudopotentials $v_\alpha(\vec{r}, 0)$ are determined through a fitting procedure. This essentially ensures that the bulk binaries described by $v_\alpha(\vec{r}, 0)$ have the experimentally available high symmetry points (Γ, X, and L) energy eigenvalues and effective masses. Other parameters, such as hydrostatic and biaxial deformation potentials, are extracted during this fitting procedure, but they are merely compared, rather than fitted, to experimental data, and are not explicitly used as such in the supercell calculations. In addition, we perform a fit of the band gap bowing parameter of the $A_xB_{1-x}C$ alloy for each AB/AC pair of binaries.

For the present calculations, we used for the screened, unstrained pseudopotentials entering Eq. (3) the expression given by Williamson et al.:[23]

$$v_\alpha(\vec{r}, 0) = \frac{1}{\Omega} \sum_{\vec{q}} e^{i\vec{q}\cdot\vec{r}} v_\alpha(q), \quad (4)$$

with

TABLE III. Parameters for the screened atomic pseudopotentials [in atomic units—see Eq. (5)] for GaSb and InSb used in this work. A plane-wave cut-off of 5 Ry was used in fitting these potentials. Also listed is the strain fitting parameter γ entering Eq. (3).

Binary:	GaSb		InSb	
	Ga	Sb	In	Sb
a_0	1221608.66	35.0805	647.2359	25.7447
a_1	1.826014	2.411019	1.757960	2.411360
a_2	41060.34	1.236884	8.714475	1.209523
a_3	0.239676	0.468184	0.677514	0.368284
a_{SO}	2.39×10^{-6}	0.355028	5.557×10^{-5}	0.542946
γ	2.029840	0.00000	1.133162	0.00000

$$v_\alpha(q) = a_{0,\alpha} \frac{q^2 - a_{1,\alpha}}{a_{2,\alpha} e^{a_{3,\alpha} q^2} - 1}. \qquad (5)$$

The material and atom specific parameters for InAs, GaAs, InP, GaP, and their alloys are the same as those given in Refs. 2, 23, and 24, while for InSb and GaSb we used the values provided in Table III.

A comparison of the fitted (PP) values with the experimental ones ("target values") used during the fitting procedure is given in Table IV. As can be seen from this table, a satisfactory agreement between the experimental and fitted data could

TABLE IV. Fitted bulk electronic properties for GaSb and InSb using the screened atomic PP derived in this work and listed in Table III. All energies are given relative to the unstrained $E_{\Gamma_{15v}}$ of the respective material. m_e^*, m_{hh}^*, m_{lh}^* are the effective masses for the electron, the heavy-hole, and the light-hole; $a_{\Gamma_{1c}}$, $a_{\Gamma_{15v}}$ are the hydrostatic deformation potentials at the Γ_{1c} and Γ_{15v} edges; b is the biaxial deformation potential; Δ_0 is the spin-orbit splitting of Γ_{15v}.

Binary:	GaSb		InSb	
Property	PP	Target	PP	Target
$E_{\Gamma_{15v}}$ (eV)	−5.043	−5.049[a]	−5.043	−5.039[a]
$E_{\Gamma_{1c}}$ (eV)	0.806	0.811[b]	0.233	0.235[b]
$E_{X_{1c}}$ (eV)	1.134	1.141[b]	1.808	1.790[b]
$E_{X_{3c}}$ (eV)	1.318	1.500[c]	1.832	1.860[c]
$E_{X_{5v}}$ (eV)	−2.712	−2.860[c]	−2.138	−2.400[c]
$E_{L_{1c}}$ (eV)	0.889	0.897[b]	0.954	0.930[b]
$E_{L_{3v}}$ (eV)	−1.127	−1.100[c]	−0.907	−1.400[c]
$m_e^*(\Gamma)$	0.041	0.042[b]	0.015	0.014[b]
$m_e^*(X_{1c,l})$	1.590	1.510[b]		
$m_e^*(X_{1c,t})$	0.168	0.2200[b]		
$m_{hh}^*[100]$	0.264	0.267[b]	0.355	0.230[b]
$m_{hh}^*[111]$	0.626	0.780[b]	0.476	0.265[b]
$m_{lh}^*[100]$	0.048	0.050[b]	0.016	0.016[b]
$a_{\Gamma_{1c}}$	−6.296	−8.01[d]	−8.148	−7.70[e]
$a_{\Gamma_{15v}}$	−1.422	−1.32[e]	−0.951	−1.10[e]
b	−2.174	−2.00[b]	−2.376	−2.00[b]
Δ_0 (eV)	0.693	0.752[b]	0.952	0.803[b]

[a]Reference 25.
[b]Reference 26.
[c]Reference 27.
[d]Reference 28.
[e]Reference 29.

be achieved. Particular care has been taken here to ensure the consistency of these potentials with the previously determined pseudopotentials[23,24] for the rest of the III-V binaries, by taking the same kinetic energy scaling factor $\beta = 1.23$ [see Eq. (2)] and energy cut-off 5 Ry, and fitting the band gap bowing parameter for all possible ternary alloys.

C. Solving the single-particle pseudopotential Schrödinger equation

We determine the QD eigenstates $\{E_i, \psi_i(\vec{r})\}$ by solving the single-particle equation, Eq. (2), using a basis set for $\psi_i(\vec{r})$ which consists of a strain-dependent linear combination of bulk bands (LCBB)[30] $u_{\nu,\vec{k}}^\lambda(\vec{r}, \varepsilon)$, of band index ν and wave vector $\vec{k}$ of the various materials λ forming the QD system. This linear combination is not restricted to bulk bands originating from Γ-valley only, but may also include X- or L-valley bulk states. This allows us to precisely identify QD states that might originate from an inter-valley coupling. Strain modifications were accounted for both in the QD and in the matrix materials, whenever applicable. We note here that this is an additional strain dependence, introduced in the basis functions, which is separate from the appropriate strain modifications of the atomic pseudopotentials in Eq. (3).

In the case of a biaxially strained, that is, not identical with the substrate, or an alloyed matrix, an additional calculation is performed to determine its CB/VB edges. These correspond to the "far-from-QD" material and define the fundamental band gap of the QD-matrix-WL system. In case of an alloy, we solve Eq. (2) using a plane-wave ansatz, adopting a supercell approach and a spectral analysis methodology[31,32] for a number of 12 random realizations of the matrix alloy.

IV. STRAIN BALANCE CONDITION AND ITS DETERMINATION

A fundamental problem in the implementation of the QD-IBSC is the requirement of ensuring a large number of QD layers in the cell. This is needed for at least two reasons: (i) a reasonably large amount of radiation has to absorbed within the QDs; and (ii) a significant number of QDs need to lie in the flat-band region of the cell and act as IB absorbers.[33] Yet, by its very nature, QD formation leads to the inherent accumulation of strain along the growth direction, strain that needs to be relieved in order to prevent adverse associated effects, like the occurrence of defects and formation of recombination centers, QD size increase, and intermediate band widening.

The problem of strain accumulation in large superlattices may be circumvented using the concept of strain-balance or strain symmetrization.[2,34,35] This leads to significant improvement of QD-IBSC characteristics: higher photocurrent, open circuit voltage, and fill factor could already been demonstrated.[2,6,10,11,36]

The basic idea is illustrated in Fig. 2(a) and can be described as follows: given a substrate with lattice constant a_0 on which a film of thickness t_{film} and natural lattice constant $a_{film} < a_0$ needs to be grown, what is the lattice constant a_{mat} and the thickness t_{mat} of a buffer layer needed,
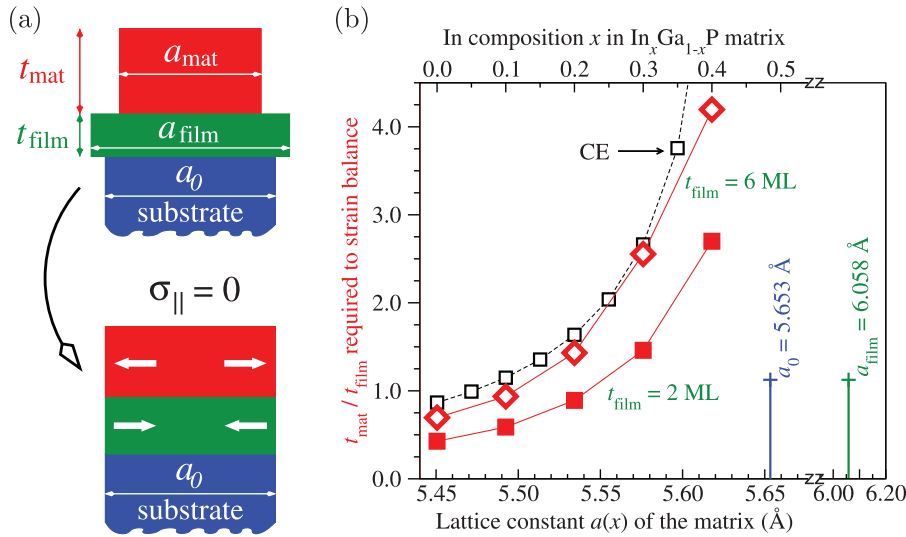
FIG. 2. (a) Illustration, for a quantum well (QW) on a substrate of lattice constant a_0, of the principle of strain balance: an appropriate tensile-compressive strain combination of the two materials forming the QW ($a_{film} > a_0$) and the matrix ($a_{mat} < a_0$) needs to be found, such that, by appropriately choosing the thickness ratio t_{mat}/t_{film}, the in-plane stress is zero. (b) Results of simulations, using atomistic elasticity, Eq. (6) [red (gray) thick symbols] for an InAs/(In,Ga)P QW of thickness 2 (squares) and 6 (diamonds) monolayers. The results are compared with those obtained using CE which are independent on the thickness t_{film}.

such that the sequence of tensile-compressive strain—$a_{film} < a_0 < a_{mat}$—leads to zero overall in-plane stress?

We briefly revisit in this section two methods of strain balance determination, using atomistic and continuum elasticity (AE and CE). We show, with a specific example of an InAs/(In,Ga)P quantum well system, that, in many cases, the CE results are not completely reliable, since this method is too "far sighted," missing significant contributions of interatomic coupling in the limit of thin layers.

A. Determining the strain balance condition with atomic resolution

In order to predict the desired geometry, that is, the appropriate t_{mat}/t_{film} ratio, one has to calculate the elastic strain energy $E = UV$ of the epitaxial combination of the two materials, where V is the volume of the sample. The stress and strain tensors $\underline{\sigma}$ and $\underline{\varepsilon}$ are related by

$$\underline{\sigma} = \frac{\partial U}{\partial \underline{\varepsilon}} = \frac{1}{V}\frac{\partial E}{\partial \underline{\varepsilon}}. \tag{6}$$

Choosing a frame of reference with its z-axis along the growth direction, the in-plane components of the stress tensor $\underline{\sigma}$ can be calculated after imposing the condition that the system is relaxed along z, i.e., that the surface and all the interfaces are stress-free.[2]

Here, we calculate directly the elastic energy E and the density U on an atomistic level by making use of the VFF functional, Eq. (1). From this, the stress tensor $\underline{\sigma}$ can be obtained by numerical evaluation of the energy gradient entering Eq. (6). For a given film material (fixed lattice constant a_{film} and thickness t_{film}), one varies the composition and thickness of the matrix material evaluating, at each point, the resulting in-plane stress. Determining the zeros of this quantity provides the thickness t_{mat} corresponding to a strain-balanced t_{mat}/t_{film} combination.

B. Application of atomistic strain balance determination to InAs/InGaP/GaAs(001) quantum well

The CE provides a relatively simple, alternative way to evaluate the elastic energy and its density entering Eq. (6).

As shown by various authors,[2,34,35] the CE-derived strain balance condition only depends on the elastic coefficients of the two materials involved. For the (001) direction, this condition reads

$$\frac{t_{mat}^{(001)}}{t_{film}^{(001)}} = -\frac{A_{film}^{(001)}\,\varepsilon_\|(film)\,a_{mat}}{A_{mat}^{(001)}\,\varepsilon_\|(mat)\,a_{film}}, \tag{7}$$

where

$$\varepsilon_\|(\alpha) = \frac{a_0 - a_\alpha}{a_0} \quad \text{for} \quad \alpha \equiv \text{film or mat}, \tag{8}$$

and

$$A_\alpha^{(001)} = C_{11,\alpha} + C_{12,\alpha} - \frac{2C_{12,\alpha}^2}{C_{11,\alpha}} \quad \text{for (001)}, \tag{9}$$

with $C_{11,\alpha}$, $C_{12,\alpha}$ the elastic constants of the film and matrix materials. Obviously, the strain balance ratio of Eq. (7) shows no thickness dependence of the constituents (film or matrix) in its right-hand side.

We compare here AE and CE determination of the strain balance condition for an InAs quantum well (QW) deposited on a GaAs(001) substrate embedded in an (In,Ga)P alloy matrix. The thickness of the QW is kept fixed while the composition and the thickness of the barrier are sought for the strain balance condition appropriate to each QW thickness. Our results are shown in Fig. 2(b) where the corresponding lattice constants of the QW and the substrate are also indicated, labeled by vertical bars. The way the results of such calculations are to be interpreted is the following: one picks a certain QW thickness, e.g., 2 MLs, and reads, from the top axis, a desired composition x of the In$_x$Ga$_{1-x}$P matrix. The corresponding ordinate of the 2 ML curve provides the ratio t_{mat}/t_{film} for which the two layers are at strain balance condition. Using the matrix lattice constant determined this way, in conjunction with that of the substrate and of the film, allows a direct estimation of the in-plane strain. The basic principle of strain balance becomes now obvious: at a fixed film-substrate compressive strain, the smaller the tensile

strain of the matrix, the thicker this needs to be to compensate for the compressive stress.

We find that the AE results [red (gray) squares and diamonds for 2 and 6 ML thick QWs] strongly depend on the actual thickness of the QW, a feature that cannot be captured by CE, results shown by open squares in Fig. 2(b). On the other hand, inspection of Fig. 2(b) clearly demonstrates that, for a 6 ML QW, the AE values are closer to the CE predictions. This is a clear indication of CE failing to describe properly the thin-thickness domain, where inter-atomic coupling extends over a range comparable to the actual thickness of the layers. Finally, we need to emphasize here that the atomistic approach can be readily applied to nanostructures of any shape.

V. EXPLORING DIFFERENT MATRIX MATERIALS

In this section, we study different choices of matrix materials, using as dot material InAs. We will compare the results with the InAs/GaAs/GaAs(001) benchmark. Its electronic levels diagram is shown, for what we define as standard geometry (lens-shaped dot, diameter 25 nm, height 3.5 nm) in Fig. 3(a). As can be seen in this figure, the IB position is expected to be about 0.31 eV below the GaAs CBM and separated by $\simeq 1.01$ eV from the highest occupied (confined) level. Comparison with the target values ($E_L = 0.7$ eV and $E_H = 1.2$ eV) (see Fig. 1) reveals how far this benchmark system is from the ideal case.

The expected open circuit voltage deduced from the theoretical results is $V_{oc} = E_L + E_H \simeq 1.32$ with $E_L = 1.01$ eV. One of the biggest promises of the IBSC concept is that of an enhancement of the short-circuit current J_{sc}—stemming from sub-band gap transitions—*without* any loss in V_{oc}. As found in various experiments, however, this did not happen, in any of the structures investigated.[5–11,37] It is now commonly accepted that one of the most important sources of this loss in V_{oc} is the presence of localized defects in the cell.[5,7] This emphasizes on the important role the matrix

might be playing in the realization of a good performing QD-IBSC: (i) an increased fundamental band gap of the matrix can preserve a relatively high V_{oc} even in the presence of such inherent losses; (ii) a less strained matrix, on the other hand, even with a smaller band gap may show a diminished loss; (iii) last but not least, if a higher CB offset is achieved, this will lead to an increase of ΔE_c, thus reducing the deleterious carrier recombination between the CB and the IB.

We show in Figs. 3(b)–3(d) some possible matrix realizations, without changing the dot or the substrate material. The calculation of QD and matrix eigenvalues followed the recipe described in Sec. III C, with a separate evaluation, where appropriate, of the strained alloy matrix band edges. In analyzing the results, we discuss the implications on the "target energy levels" $\Delta E_c \equiv E_L$ (electron levels offset—light blue/gray arrow), inter-band intra-dot transition (black arrow), matrix band gap $E_g = E_L + E_H$, and ΔE_v (hole levels offset—green/dark gray arrow) that need to evolve as discussed in Sec. II. This pattern and results layout will be used also in the subsequent sections. For the matrix material variation, our results can be summarized as follows:

(A) $In_{0.2}Ga_{0.8}As$ *matrix [Fig. 3(b)]*: this system has been already experimentally realized[38] and showed to have benefic influence on the quality of the InAs QDs, because of the strain relieving role of the $In_{0.2}Ga_{0.8}As$ matrix in the structure. Our calculations show, however, that while ΔE_v decreases as compared to InAs/GaAs QD (positive effect), other parameters, such as the electron levels offset, $\Delta E_c = 0.21$ eV, and the matrix band gap, $E_g = 1.33$ eV, exhibit a not desired evolution, and thus do not recommend this system as a QD-IBSC candidate.

(B) $GaAs_{0.8}Sb_{0.2}$ *matrix [Fig. 3(c)]*: Also this system has been realized experimentally and the results discussed in conjunction with eight band $\vec{k} \cdot \vec{p}$ calculations.[12,13] Addition of Sb during growth has been found to increase the QD density and reduce both the spread as well as the overall QD dimensions. As a result, the photoluminescence (PL) peak becomes narrower in InAs/Ga(As,Sb) QDs, for a nominal Sb composition

Dot (*h*/nm):	(a) InAs (3.5)	(b) InAs (3.5)	(c) InAs (3.5)	(d) InAs (3.5)
Matrix:	GaAs	In$_{0.2}$Ga$_{0.8}$As	GaAs$_{0.8}$Sb$_{0.2}$	In$_{0.3}$Ga$_{0.7}$P
Substrate:	GaAs (001)	GaAs (001)	GaAs (001)	GaAs (001)
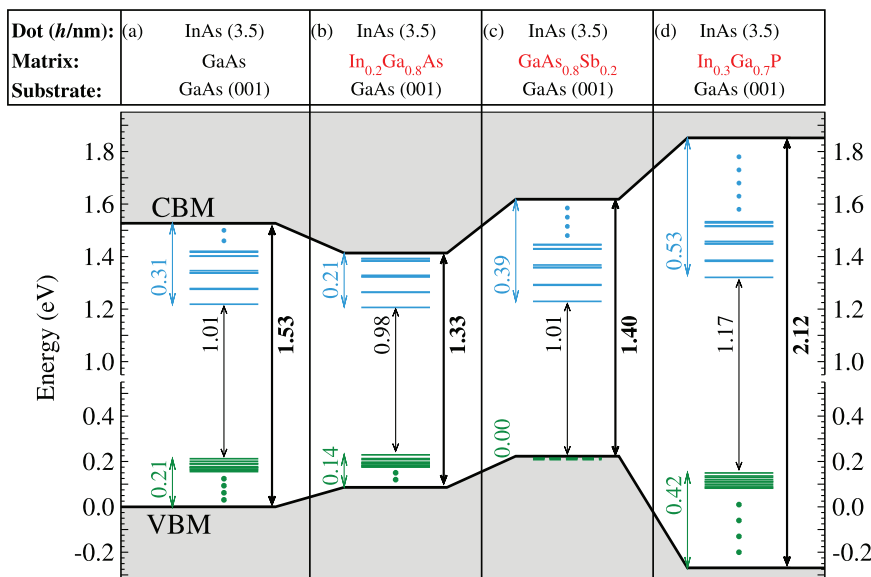
FIG. 3. Calculated single-particle energy levels for several QD-IBSC systems consisting of an InAs lens-shaped dot, diameter 25 nm and height 3.5 nm embedded in various matrices on GaAs(001) substrate. The energy zero corresponds to GaAs VBM. Only the first ten (Kramers degenerate) levels are shown for electrons and holes.

of 23 at. %. Contrary to the expectations, the QDs size reduction is accompanied by a red-shift of the PL peak. This reduction of the HOMO-LUMO separation is mainly due to a raise in energy of the initial (hole) state. Indeed, our calculations for epitaxially strained $GaAs_{0.8}Sb_{0.2}$ alloy shows a 0.21 eV upwards shift of the VBM as compared to GaAs. As a consequence, the InAs hole states are now energetically below the Ga(As,Sb) matrix VBM. This result is in agreement with the $\vec{k} \cdot \vec{p}$ results of Ban et al.[13] who also obtain a zero hole levels offset ΔE_v, a very encouraging result for IBSC. As can be seen in Fig. 3(c), also $\Delta E_c = E_L$ is increased, 0.39 eV, as compared to the benchmark system InAs/GaAs. This is caused by the higher energy (on an absolute scale) of the CBM in the strained $GaAs_{0.8}Sb_{0.2}$ as compared to GaAs. The single-particle HOMO-LUMO separation (corresponding to E_H) for $InAs/GaAs_{0.8}Sb_{0.2}$ QD we obtained is 1.01 eV, showing no change versus InAs/GaAs. In contrast, the calculations of Ban et al.[13] give a 1.14 eV value, slightly higher than ours. From the point of view of IBSC functionality, two negative aspects need to be mentioned: (i) the band gap of the matrix (1.40 eV) and thus the expected V_{oc} is smaller than in GaAs, and (ii) on a GaAs(001) substrate, both the QD and the matrix are introducing a compressive strain that might accelerate the detrimental strain accumulation when several QD layers need to be grown.

(C) *InAs QD in $In_{0.3}Ga_{0.7}P$ matrix [Fig. 3(d)]*: Extremely popular in photovoltaics, this alloy has not yet been studied as potential matrix for a QD system. Known as exhibiting a wide band gap, our calculations show that even under the biaxial strain of the GaAs(001) a large, 2.12 eV, direct band gap can be expected. Despite the hole levels offset being high, 0.42 eV, that would reduce the open circuit voltage, we expect a QD-IBSC based on $InAs/In_{0.3}Ga_{0.7}P/GaAs(001)$ to show improved solar cell characteristics versus the benchmark system. Indeed, such expectations seem to be justified by comparing the increased $E_H = 1.17$ eV value for the intra-dot transition, the increased

$E_L = \Delta E_c = 0.53$ eV, and the theoretical $E_L + E_H = 1.70$ eV for this system with the corresponding values of InAs/GaAs. Moreover, amongst the systems studied, these numbers come in closest agreement to the ideal E_L and E_H values of Luque and Martí[1] of $\simeq 0.7$ eV and $\simeq 1.2$ eV, respectively. In addition, as shown in Sec. IV B, these materials combination is also suited for strain-balance engineering, which might improve the morphology of the grown cells. The biggest challenge that needs to be overcome, however, is the relatively difficult growth process of both InAs and InP-based systems.[39]

The calculations presented in this section show that the influence of the matrix on the position of the such formed IB is mainly due to relative shifts of the CBM/VBM edges of the matrix, caused by alloying and/or biaxial strain. The modifications in the matrix band edges obviously change both the fundamental band gap as well as the reference values for ΔE_c and ΔE_v. An even more subtle influence is related to the change in the electron and hole confinement, since the matrix CBM and VBM serve as binding reference level for the potential wells formed by the QDs. This effect is expected to be even stronger when the QD material is changed.

VI. EXPLORING DIFFERENT DOT MATERIALS

In modeling the QD-IBSC systems, the IB is considered to be formed by the deepest QD-confined levels (electrons or holes). We note that, for typical self-assembled QD systems, the biaxial strain is compressive for the QD materials, which effectively leads to a significant reduction of the confining potential well as compared to the unstrained situation. We focus here on the effects on the IB position (and the derived target parameters $E_L = \Delta E_c$, E_H and ΔE_v) by changes in the QD material. Our results are summarized in Fig. 4 where, in panel (a), we carry over the energy level diagram of the benchmark system InAs/GaAs/GaAs(001).
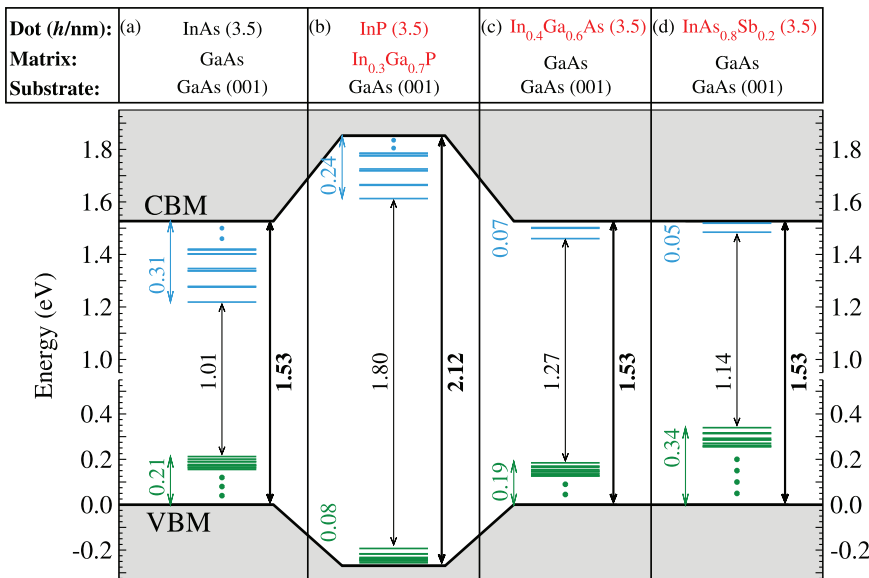
FIG. 4. Same as Fig. 3 but with various QD materials.

(D) InP QD in In$_{0.3}$Ga$_{0.7}$P matrix [Fig. 4(b)]: This system is a variation of system (C) discussed above which, as we could see, along with certain promising features like a wide band gap and a large $\Delta E_c = E_L$, also exhibits an inconveniently large ΔE_v (hole levels offset) that drastically reduces the open circuit voltage V_{oc}. The use of InP as a QD material may appear justified by the fact that the valence band offset between InP and GaP is relatively small, the InP VBM lying 0.11 eV above that of GaP.[25] As can be seen in Fig. 4(b), the expectation on a decreasing ΔE_v is fulfilled, as this value becomes 0.08 eV, much smaller than in the (C)-system, InAs/In$_{0.3}$Ga$_{0.7}$P, which has $\Delta E_v = 0.42$ eV. Unfortunately, the price paid for this improvement in the hole levels offset is an equally dramatic decrease of ΔE_c down to 0.24 eV—from 0.53 eV in system (C)—being even worse than the benchmark system InAs/GaAs. Altogether, the prognosis for such a system is by far poorer than for the close to ideal system (C).

(E) In$_{0.4}$Ga$_{0.6}$As QD in GaAs matrix [Fig. 4(c)]: In order to reduce the effect of strain accumulation, one might be tempted to chose an alternative path to either strain balance or the insertion of strain relieving layers [e.g., system (B)] by alloying the dot material and thus to reduce the compressive strain. For an InAs QD embedded in GaAs, the most direct way to do this is by substituting for In with Ga, which significantly reduces the mismatch between dot and matrix (and also substrate). As shown by our results for In$_{0.4}$Ga$_{0.6}$As/GaAs/GaAs(001) in Fig. 4(c), this has negative influences on the IBSC characteristics. Compared to the pristine InAs/GaAs system, there is nearly no change in ΔE_v, which only decreases by 20 meV, but the electron levels offset ΔE_c is strongly diminished, reaching 0.07 eV. Previous investigations on such alloyed (In,Ga)As QDs[40] revealed that geometrical or composition variations in the QDs do not significantly change this small value of ΔE_c.

(F) InAs$_{0.4}$Sb$_{0.6}$ QD in GaAs matrix [Fig. 4(d)]: A reduced electron levels offset ΔE_c is not necessarily detrimental for a potential IBSC, provided that, by a corresponding significant increase of the hole levels offset ΔE_v, their role is basically switched. This is equivalent to the IB being formed by the deep confined *holes*, unlike the systems surveyed so far in which the electron levels were assumed to form the IB. In such a case, ΔE_v plays the role of E_L while E_H is measured from the IB (now formed by holes) to the CBM of the matrix. Examples of such systems are the GaSb/GaAs QDs[16] that have been already shown to exhibit a sub-band gap contribution to the quantum efficiency or the recently emerging In(As,Sb)/GaAs QD systems[14,15] which can be seen as dot-modified versions of the current InAs/GaAs benchmark. It has been shown[14,15] that, upon Sb inclusion into the InAs QD, a type I to type II transition occurs at a composition, estimated by $\vec{k} \cdot \vec{p}$ simulations, of 60% Sb. These findings could be confirmed experimentally by PL measurements.[14]

Results of our atomistic calculations for the lens-shaped, 3.5 nm tall and 25 nm wide InAs$_{0.4}$Sb$_{0.6}$ QD in GaAs are shown in Fig. 4(d). As can be seen, the electron levels offset is quite small, 0.05 eV, that is, our system (still type I), is close to the type II transition. Since the IB is now formed by the hole levels, $\Delta E_v = E_L$ needs to be compared with ΔE_c in

InAs/GaAs QDs. One finds a slight increase, 0.34 eV versus 0.31 eV, which would be favorable for the IBSC. Since the matrix is identical to the benchmark system, the band gap is the same, leading to the conclusion that In(As,Sb)/GaAs QDs close to the type I to type II transition should be at least as good candidates as InAs/GaAs for a QD-IBSC implementation. As it is true also for the GaSb/GaAs QDs, however, legitimate concerns arise from the viability of such a "hole-levels generated" IB: indeed, the density of the hole levels is much higher than that of the electron levels; typically, in a QD the confined hole levels are separated by $\simeq 1$ meV, whereas the electron levels, at identical QD sizes, show a $\simeq 10$ meV separation. Nevertheless, in combination with appropriate substrates (see below) and with an enhanced matrix band gap (e.g., by alloying with Al), there are certain interesting features that make the Sb-based systems promising IBSC candidates.

VII. EXPLORING COMBINATIONS OF DOT-MATRIX-SUBSTRATE THAT LEAD TO STRAIN BALANCE

The advantages opened using strain balance (or strain compensating) systems have been discussed in detail in Sec. IV. One currently distinguishes between two main trends concerning its application; first idea is to introduce thin strain-compensating layers, different from the matrix itself, e.g., GaP or Ga(As,P) in GaAs.[6,7,36] The second is to create a strain compensating matrix *in integrum*, by appropriate alloying with the desired composition such as to attend a targeted strain, opposed to the (usually compressive) one created by the QDs. Examples for such systems are the Ga(As,N) dilute alloy used by Okada *et al.*[10,11] and the GaAs$_{0.86}$P$_{0.14}$ alloy in conjunction with In$_{0.47}$Ga$_{0.53}$As QDs.[2] It appears, however, that the insertion of strain compensating layers effectively introduces additional potential barriers in the path of the extracted carriers, similar to the unfavorable side effect of the "fence" layers.[8,37] Regardless of the method used, however, the recipe necessarily requires an adequate combination of all three ingredients: QD, matrix, and substrate.

We show in Fig. 5 energy levels for three of these combinations and compare them again with the InAs/GaAs benchmark [depicted in panel Fig. 5(a)]. One of these, InAs QD in In$_{0.3}$Ga$_{0.7}$P on GaAs(001), has been already discussed in detail [system (C) above, shown in Fig. 5(b)], while a second one, In$_{0.47}$Ga$_{0.53}$As/GaAs$_{0.86}$P$_{0.14}$/GaAs(311B), Fig. 5(d), made the subject of one of our early investigations.[2] This QD-matrix-substrate combination, although of excellent quality, showed no improved IBSC characteristics, for the obvious reasons revealed by Fig. 5(d): while the band gap of the matrix is practically the same as that of GaAs, ΔE_c is significantly lower than in the benchmark system.

Here, we introduce a new system, with a good potential for achieving strain balance, a modification of system (B) that uses InP(001) as substrate, material which is nearly perfectly lattice matched with GaAs$_{0.51}$Sb$_{0.49}$.[26] We note that here we turn back to the situation in which the IB is formed by the QD confined electron levels.
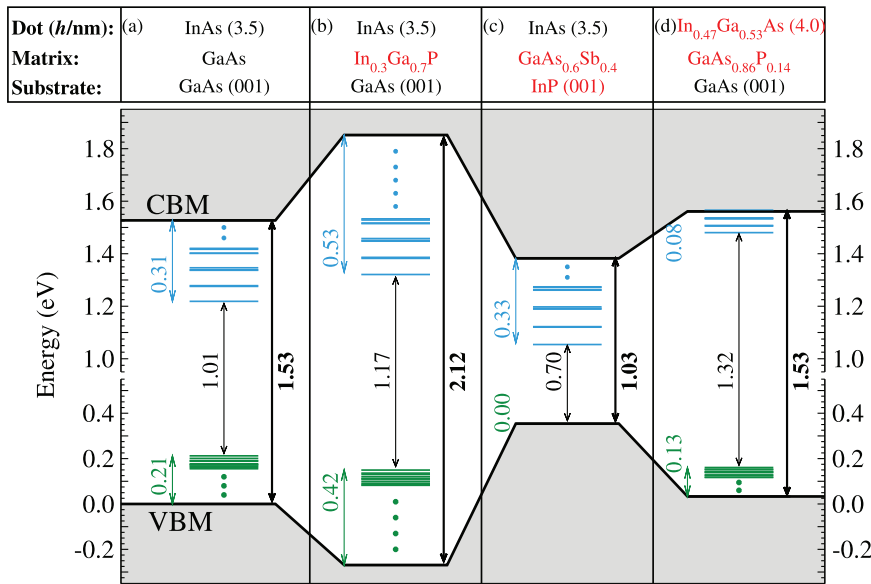
FIG. 5. Same as Fig. 3 but with QD-matrix-substrate combinations that allow strain balanced structures.

(G) InAs QD in GaAs$_{0.6}$Sb$_{0.4}$ matrix on InP(001) substrate [Fig. 5(c)]: As a result of the biaxial strain, the VBM of GaAs$_{0.6}$Sb$_{0.4}$ on InP(001) is lifted as compared to Ga(As,Sb) on GaAs(001). This leads to a similar beneficial effect as for the InAs/Ga(As,Sb) system (B): the hole levels offset ΔE_v is zero. Another positive aspect of this system is that the electron levels offset remains practically of the same size as in InAs/GaAs. A serious problem, however, is the low predicted value, 1.03 eV, of the band gap E_g of the Ga(As,Sb) under biaxial strain. An alternative to remove this inconvenience might be provided by the alloying of the matrix, e.g., with Al, and thus enhancing the band gap of the matrix.

VIII. CONCLUSIONS

Taking a prototype geometry for a QD-matrix-substrate system, we have calculated the energy level alignments for a series of III-V compounds and alloys and evaluated their potential to provide the desired offsets required for a QD-IBSC implementation. In doing so, we used a multi-band atomistic pseudopotential approach, with a high level of accuracy and prediction ability. Our investigations started from a widely used QD-IBSC benchmark system, InAs/GaAs, and analyzed the evolution of the relevant energy differences: band-gap, electron, and hole level offsets, HOMO-LUMO separation, upon compositional changes of the (i) dot and (ii) matrix materials. We surveyed some of the "usual suspects" amongst the III-V systems and compared their electronic structure against that of the benchmark system as well as from the point of view of the ideal case of a maximum efficiency. In addition, we have performed atomistic elasticity calculations for an InAs/(In,Ga)P/GaAs(001) quantum well to determine the strain balance condition for such a structure. These results have shown that the simple methodology provided by continuum elasticity is limited in validity for the case of thin layers.

Our investigations have shown that, technological difficulties notwithstanding, some QD-matrix-substrate systems could make the subject of more detailed experimental and theoretical investigations owing to their positive prognosis for a QD-IBSC realization. The systems we found to fulfill these characteristics are (in QD/matrix notation):

(i) In(As,Sb)/GaAs with the IB formed by the dot-confined holes and positioned 0.34 eV above the GaAs VBM. With an adequate choice of the substrate the system could be strain balanced, while matrix alloying with Al may lead to an increase of the main band gap.

(ii) InAs/In$_{0.3}$Ga$_{0.7}$P with the IB formed by dot-confined electron levels, and with a wide, direct band-gap matrix. We have shown, by AE calculations, that such a material combination can be strain balanced on a GaAs(001) substrate. Moreover, the matrix remains a direct band gap semiconductor even under this biaxial strain. From all the investigated systems, these QD-matrix-substrate combinations came to the closest agreement with the E_L/E_H values prescribed for the ideal maximum efficiency under concentrated radiation.

(iii) InAs/GaAs$_{0.6}$Sb$_{0.4}$/InP(001) is yet another system with a potential for strain balance exhibiting a zero hole levels offset. This is equivalent to no "energy offset caused" loss in the open circuit voltage, which, in turn, could be enhanced by appropriate alloying of the matrix.

We have restricted our study to a quite common class of semiconductors, formed by the III-V group elements. Without exhausting all possibilities, our calculations have shown that, while several combinations appear to be quite promising, it is nevertheless necessary to extend the search for appropriate QD-IBSC materials beyond this class. Targeting solely the desired characteristics mentioned here—appropriate energy level alignment and preventing large strain accumulation in QD stacks—a minimum set of design principles can be summarized as follows: (a) the materials forming the substrate, the QD, and the matrix should enable strain balance engineering. In particular, their natural lattice constants need to be in the relation $a_{\text{matrix}} < a_{\text{substrate}} < a_{\text{QD}}$ in order to create a tensile-compressive strain compensating sequence; (b) the VB offset between matrix and QD materials should be small,

ideally zero *after* strain-induced band edge effects have been taken into account. In this context, it is worth mentioning that, regardless of the sign of the biaxial strain (tensile or compressive), the splitting of the Γ_{15v} level *always* leads to a raise of the VBM, whether it is the light or the heavy hole; (c) the matrix material band gap E_g needs to be as close as possible to the ideal value $E_L + E_H$. An interesting aspect requiring further investigations is related to its nature, whether direct or indirect. Whereas a direct band gap will certainly be favorable for the absorption processes into the CB [A and C in Fig. 1(a)], an indirect band gap has the advantage of a significantly slower recombination CB → IB and CB → VB. A mixture of these two characters (direct and indirect) might be a good compromise for the IBSC functionality; (d) finally, the QD material should have its CBM at a position at least half E_g (matrix band gap) below the matrix CBM. This is necessary because the combined effect of compressive strain and confinement will lead to a raise in the electron levels of the QD, typically formed by Γ-like bulk states.

The design rules given above can be readily followed using the data available in the literature,[25,26,41] and applying simple models (e.g., Pikus-Bir, continuum elasticity) common to device modeling. While the actual realization of a fully functional QD-IBSC device, remains a tremendous challenge, it is nevertheless important that detailed high-quality, atomistic calculations, able to give reliable estimates of the band alignment, absorption spectra and radiative lifetimes should further be used to complement the technological efforts.

[1]A. Luque and A. Martí, Phys. Rev. Lett. **78**, 5014 (1997).
[2]V. Popescu, G. Bester, M. C. Hanna, A. G. Norman, and A. Zunger, Phys. Rev. B **78**, 205321 (2008).
[3]S. P. Bremner, M. Y. Levy, and C. B. Honsberg, Appl. Phys. Lett. **92**, 171110 (2008).
[4]A. Luque, A. Martí, N. López, E. Antolín, E. Cánovas, C. Stanley, C. Farmer, L. J. Caballero, L. Cuadra, and J. L. Balenzategui, Appl. Phys. Lett. **87**, 083505 (2005).
[5]A. Martí, N. López, E. Antolín, E. Cánovas, A. Luque, C. R. Stanley, C. D. Farmer, and P. Díaz, Appl. Phys. Lett. **90**, 233510 (2007).
[6]S. M. Hubbard, C. D. Cress, C. G. Bailey, R. P. Raffaelle, S. G. Bailey, and D. M. Wilt, Appl. Phys. Lett. **92**, 123512 (2008).
[7]C. G. Bailey, D. V. Forbes, R. P. Raffaelle, and S. M. Hubbard, Appl. Phys. Lett. **98**, 163105 (2011).
[8]K. A. Sablon, J. W. Little, K. A. Olver, Z. M. Wang, V. G. Dorogan, Y. I. Mazur, G. J. Salamo, and F. J. Towner, J. Appl. Phys. **108**, 074305 (2010).
[9]R. Oshima, A. Takata, and Y. Okada, Appl. Phys. Lett. **93**, 083111 (2008).
[10]Y. Okada, R. Oshima, and A. Takata, J. Appl. Phys. **106**, 024306 (2009).
[11]Y. Okada, T. Morioka, K. Yoshida, R. Oshima, Y. Shoji, T. Inoue, and T. Kita, J. Appl. Phys. **109**, 024301 (2011).
[12]K.-Y. Ban, S. P. Bremner, G. Liu, S. N. Dahal, P. C. Dippo, A. G. Norman, and C. B. Honsberg, Appl. Phys. Lett. **96**, 183101 (2010).
[13]K.-Y. Ban, W.-K. Hong, S. P. Bremner, S. N. Dahal, H. McFelea, and C. B. Honsberg, J. Appl. Phys. **109**, 014312 (2011).
[14]J. He, C. J. Reyner, B. L. Liang, K. Nunna, D. L. Huffaker, N. Pavarelli, K. Gradkowski, T. J. Ochalski, G. Huyet, V. G. Dorogan *et al.*, Nano Lett. **10**, 3052 (2010).
[15]Y. I. Mazur, V. G. Dorogan, G. J. Salamo, G. G. Tarasov, B. L. Liang, C. J. Reyner, K. Nunna, and D. L. Huffaker, Appl. Phys. Lett. **100**, 033102 (2012).
[16]R. B. Laghumavarapu, A. Moscho, A. Khoshakhlagh, M. El-Emawy, L. F. Lester, and D. L. Huffaker, Appl. Phys. Lett. **90**, 173125 (2007).
[17]K. A. Sablon, J. W. Little, V. Mitin, A. Sergeev, N. Vagidov, and K. Reinhardt, Nano Lett. **11**, 2311 (2011).
[18]A. Zunger, Phys. Status Solidi B **224**, 727 (2001).
[19]V. Popescu, G. Bester, and A. Zunger, Phys. Rev. B **80**, 045327 (2009).
[20]P. N. Keating, Phys. Rev. **145**, 637 (1966).
[21]R. M. Martin, Phys. Rev. B **1**, 4005 (1970).
[22]K. Kim, P. R. C. Kent, A. Zunger, and C. B. Geller, Phys. Rev. B **66**, 045208 (2002).
[23]A. J. Williamson, L. W. Wang, and A. Zunger, Phys. Rev. B **62**, 12963 (2000).
[24]M. Gong, K. Duan, C.-F. Li, R. Magri, G. A. Narvaez, and L. He, Phys. Rev. B **77**, 045326 (2008).
[25]S.-H. Wei and A. Zunger, Appl. Phys. Lett. **72**, 2011 (1998).
[26]I. Vurgaftman, J. R. Meyer, and L. R. Ram-Mohan, J. Appl. Phys. **89**, 5815 (2001).
[27]X. Zhu and S. G. Louie, Phys. Rev. B **43**, 14142 (1991).
[28]Y.-H. Li, X. G. Gong, and S.-H. Wei, Phys. Rev. B **73**, 245206 (2006).
[29]S.-H. Wei and A. Zunger, Phys. Rev. B **60**, 5404 (1999).
[30]L.-W. Wang and A. Zunger, Phys. Rev. B **59**, 15806 (1999).
[31]V. Popescu and A. Zunger, Phys. Rev. Lett. **104**, 236403 (2010).
[32]V. Popescu and A. Zunger, Phys. Rev. B **85**, 085201 (2012).
[33]L. Cuadra, A. Martí, and A. Luque, IEEE Trans. Electron Devices **51**, 1002 (2004).
[34]N. J. Ekins-Daukes, K. Kawaguchi, and J. Zhang, Cryst. Growth Des. **2**, 287 (2002).
[35]L. Bhusal and A. Freundlich, Phys. Rev. B **75**, 075321 (2007).
[36]R. B. Laghumavarapu, M. El-Emawy, N. Nuntawong, A. Moscho, L. F. Lester, and D. L. Huffaker, Appl. Phys. Lett. **91**, 243115 (2007).
[37]G. Wei and S. Forrest, Nano Lett. **7**, 218 (2007).
[38]V. D. Dasika, J. D. Song, W. J. Choi, N. K. Cho, J. I. Lee, and R. S. Goldman, Appl. Phys. Lett. **95**, 163114 (2009).
[39]A. Norman and M. Steiner, private communication (2011).
[40]G. A. Narvaez, G. Bester, and A. Zunger, J. Appl. Phys. **98**, 043708 (2005).
[41]*Numerical Data and Functional Relationships in Science and Technology*, Landolt-Börnstein, New Series, Group III Vol. 22, edited by O. Madelung, M. Schultz, and H. Weiss (Springer, Berlin, 1997).